CRYSTAL GROWTH & DESIGN

Article

pubs.acs.org/crystal

How Short-Lived Ikaite Affects Calcite Crystallization

R. Besselink,[†] J. D. Rodriguez-Blanco,[‡,§] T. M. Stawski,[†] L. G. Benning,[†,∥,⊥] and D. J. Tobler*[,‡]

[†]German Research Center for Geosciences, GFZ, Telegrafenberg, 14473, Potsdam, Germany

[‡]Nano-Science Center, Department of Chemistry, University of Copenhagen, Copenhagen, Denmark

[§]iCRAG, Department of Geology, School of Natural Sciences, Trinity College Dublin, Dublin 2, Ireland

[∥]Department of Earth Sciences, Free University of Berlin, 12249 Berlin, Germany

[⊥]School of Earth and Environment, University of Leeds, Leeds, United Kingdom

ABSTRACT: The pathways of $CaCO_3$ crystallization are manifold, often involving one or several metastable amorphous or nanocrystalline intermediate phases. The presence of such intermediates is often overlooked, because they are short-lived and/or occur at small molar fractions. However, their occurrence does not just impact the mechanisms and pathways of formation of the final stable $CaCO_3$ phase, but also affects their crystal size, shape, and structure. Here we document the presence of a short-lived intermediate through *in situ* and time-resolved small and wide-angle X-ray scattering combined with high resolution electron microscope observations. When ikaite forms concomitant with the dissolution of amorphous calcium carbonate (ACC) but prior to calcite formation, fairly large glendonite-type calcite crystals grow despite the presence of citrate ligands that usually reduce crystal size. These were ideal seeding crystals for further crystallization from supersaturated ions in solution. In contrast, in the absence of ikaite the crystallization of calcite proceeds through transformation from ACC, resulting in fine-grained spherulitic calcite with sizes ~8 times smaller than when ikaite was present. Noteworthy is that the formation of the intermediate ikaite, although it consumes less than 3 mol % of the total precipitated $CaCO_3$, still clearly affected the calcite formation mechanism.

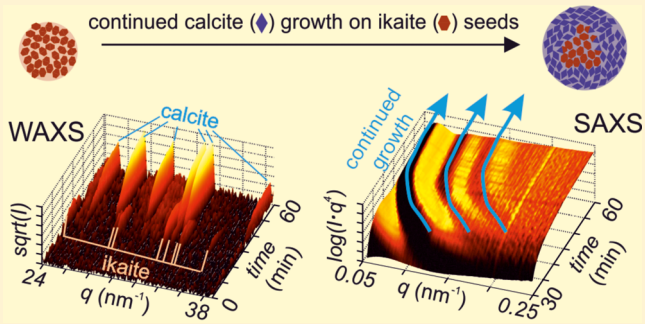

INTRODUCTION

$CaCO_3$ minerals are widespread in nature where they play a pivotal role in biomineralization processes and thus in the carbon cycle.[1] They are also important to industry where they are used for the production of paint, ceramics, paper, drugs, food supplements, abrasives, etc.[2] In many natural systems, $CaCO_3$ crystallizes as the thermodynamically most stable polymorph calcite. However, $CaCO_3$ crystallization pathways are diverse and complex because they are sensitive to many parameters, including temperature, pressure, pH, and the presence of impurities.[3−5] From a kinetic point of view, it is very difficult to form highly symmetrical and completely dehydrated calcite through a simple reaction pathway. In contrast, metastable $CaCO_3$ phases are often more easily formed, either by reduced interfacial energy of metastable phases[6] or smaller degree of dehydration required for formation.[7]

Understanding of $CaCO_3$ crystallization pathways, particularly when they involve one or more metastable precursor(s), is important because these pathways determine the size, shape, and properties of the final stable calcite (or aragonite) crystals, found in soils, sediments, and biominerals or synthesized in industrial processes. For example, when calcite forms following the breakdown of amorphous calcium carbonate (ACC), it commonly shows spherulitic morphologies.[10−14] This is explained by (1) a large solubility difference between the ACC and the crystalline polymorphs, and (2) the incorporation or adsorption of impurities blocking conventional calcite growth sites, leading to a nucleation controlled growth mechanism and formation of intertwined nanocrystals.[4,5,8,9] In contrast, when calcite forms through pseudomorphic transformation of ikaite, it exhibits the characteristic bipiramidal or hedgehog-shaped morphology of ikaite, commonly described as glendonite.[15−18] While the ikaite shape is preserved in this transformation to calcite, the molar volume is substantially reduced, by 76% (ikaite: ISCD 31305[19] and calcite: AMSCD 0000098[20]). As a result glendonites are highly porous, and they also often retain some of the ikaite structural water within the newly formed calcite crystal.[18,20]

These examples give a small glimpse into the large diversity in $CaCO_3$ crystallization pathways and show how minute changes can affect the properties of the stable end material, including porosity, grain size, mechanical strength, morphology, etc. Understanding these mechanisms at the nanoscale is key toward designing taylor-made $CaCO_3$ polymorphs for various industrial applications. Furthermore, being able to understand

Received: May 28, 2017
Revised: August 30, 2017
Published: September 19, 2017

DOI: 10.1021/acs.cgd.7b00743
Cryst. Growth Des. 2017, 17, 6224−6230

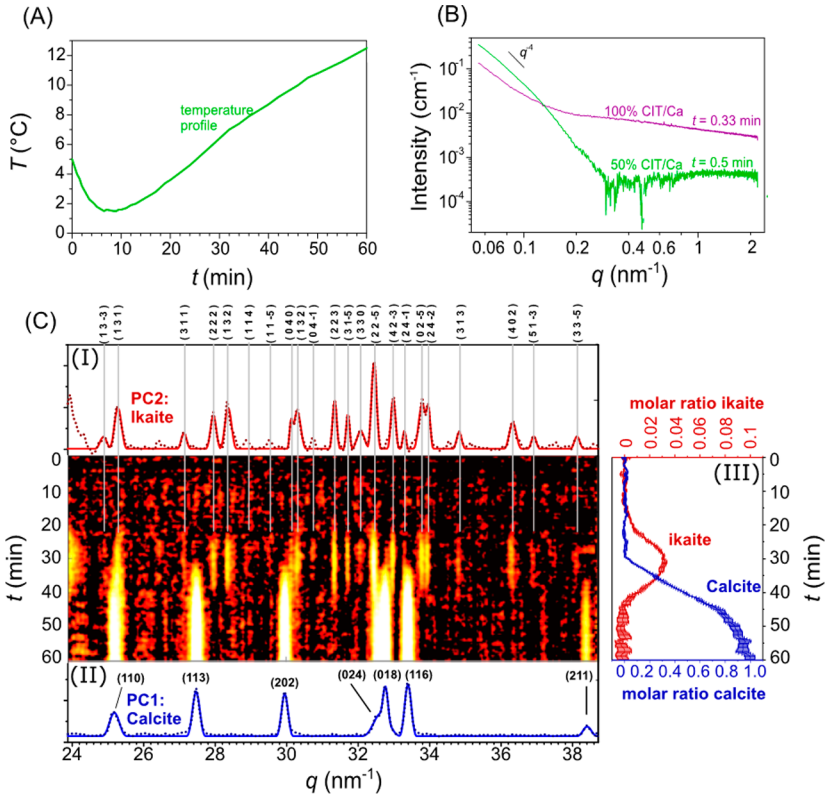

Figure 1. (A) Solution temperature as a function of experimental reaction time. (B) SAXS patterns of $CaCO_3$ suspensions 0.5 and 0.33 min after mixing for 50% and 100% CIT/Ca respectively, (C) 2D WAXS intensity map for 100% CIT/Ca with the scale increasing from black to red, orange, yellow, and white, with q-spacing (nm^{-1}) on the horizontal axis and reaction time (min) on the vertical axis. This set of WAXS scattering intensities was deconvoluted by means of principal component analysis into two characteristic patterns, namely, (I) the WAXS pattern of principal component 2 was assigned to ikaite (see Miller indices) and (II) the WAXS pattern of principal component 1 was assigned to calcite (see Miller indices), where (III) represents the time-resolved molar ratios of ikaite and calcite with respect to calcite at t = 60 min. Please note that ikaite and calcite molar ratios are scaled on separate Y-axes.

how the crystallization history is preserved in the final observed $CaCO_3$ polymorph helps to reconstruct its formation conditions. For example, porous glendonite polymorphs are paleoclimatic indicators of low-temperature condition, under which ikaite was formed.[21]

Here, we investigated the role that short-lived ikaite has during the formation of calcite via ACC by means of synchrotron based small and wide-angle X-ray scattering (SAXS/WAXS) at temperatures between 2 and 12 °C. In our previous study, we documented that in the presence of magnesium[22] or citrate,[23] ACC directly crystallizes to calcite, with no vaterite intermediate. We used here a similar setup to the above-mentioned citrate study but ran the experiments at a lower temperature to facilitate ikaite formation. We discovered that a high citrate (CIT) concentration (CIT/Ca = 100%) facilitated the formation of ikaite besides ACC, yet that this was short-lived. In contrast, at lower citrate concentration (CIT/Ca = 50%) ACC transformed directly into calcite without the ikaite intermediate. Although ikaite formation was short-lived and included <3 mol % of the total precipitated $CaCO_3$, it strongly changed the calcite crystallization mechanism and kinetics and led to the growth of far larger calcite crystals.

METHODS

The formation and crystallization of $CaCO_3$ phases were studied in the presence of citrate (CIT; $C_6H_5O_7^{3-}$) by mixing equal volumes of a 0.05 M $CaCl_2$ solution and a 0.05 M Na_2CO_3 solution with either 0.025 or 0.050 M monohydrate citric acid (corresponding to 50 or 100% CIT/Ca). Stock solutions were prepared by using reagent grade chemicals and ultrapure deionized water (Milli-Q, resistivity >18 MΩ cm). CIT-containing carbonate solutions were pH adjusted to 11.2 (2 M NaOH) to match the pH of the pure Na_2CO_3 solution. The formation and crystallization of $CaCO_3$ phases were followed *in situ* and in a time-resolved mode by using SAXS/WAXS at beamline I22 at the Diamond Light Source Ltd. (UK). For each experiment, equal volumes of the calcium and CIT-containing carbonate solution, both precooled to 5 °C, were injected into a 3-neck reactor flask (250 mL) using a remotely controlled peristaltic pump (Gilson Mini Puls 3) at 200 mL/min. The resulting mixed liquid/suspension was continuously stirred at 300 rpm and circulated at a flow rate of 50 mL/min through a flow-through cell containing a borosilicate glass capillary (d = 1.5 mm) that was aligned perpendicular to the X-ray beam. To avoid rapid warming up of the solution to the temperature of the beamline hutch (21 °C), the reactor was placed in a precooled oil bath with an initial temperature of 1 °C. After 1 h the solutions reached a temperature of 14 °C, and a typical time trend for the change in solution temperature during an experiment is shown in Figure 1A.

SAXS/WAXS data were acquired by using a monochromatic X-ray beam at 16 keV. Two-dimensional SAXS intensities were collected with a Dectris Pilatus 2M (2D large area pixel-array detector[24]). Transmission was measured by means of a photodiode installed in the beam-stop of the SAXS detector. A sample-to-detector distance of 9.22 m allowed for a usable q-range of $0.055 < q < 2.187$ nm^{-1}. The scattering range at small angles was calibrated against silver behenate[25] and dry collagen standards.[26] In all the cases the recorded 2D scattering patterns were reduced to 1D scattering curves, normalized and corrected for transmission, and background-corrected. For background subtraction we used a scattering from a cell filled with water. The intensity scale was calibrated to absolute units by using a

DOI: 10.1021/acs.cgd.7b00743
Cryst. Growth Des. 2017, 17, 6224−6230

glassy carbon ref 27. Data acquisition was performed in experiments that lasted for up to 2 h, and spectra were recorded at a time resolution of 30 s per frame.

Simultaneously, two-dimensional WAXS intensities were collected with a Decris Pilatus 300k detector (2D large-area pixel array detector,[24] which was calibrated with synthetic and highly crystalline silicon (NIST SRM 640C)). This silicon standard was used to determine the instrumental broadening ($\Delta q_{instrument} = 0.17$ nm^{-1}), and the corrected peak width ($\Delta q_{corrected}^2 = \Delta q_{measured}^2 - \Delta q_{instrument}^2$) was used to determine crystallite size by the Scherrer equation.[28] The WAXS detector covered the q-range of $23.9 < q < 38.7$ nm^{-1}. All recorded patterns were normalized and background-corrected using water. For all samples a broad correlation peak with a maximum at $q \approx 29$ nm^{-1} remained present, which we related to typical Ca−O distances within ACC: $d \approx 0.24$ nm.[23] The shape of this amorphous background was determined over the initial 10 frames, averaged, smoothed, and subtracted from the subsequent frames in the ratios individually optimized for all frames.

A principal component analysis (PCA) procedure from PTC Mathcad v15.0 was used to identify and quantify the contributions from crystalline $CaCO_3$ phases present in the time-resolved diffraction data set. This procedure allowed us to describe a large data set based on a limited set of principal components. Every principal component was represented by a vector of scores and loadings. The score vectors represent characteristic diffraction patterns of a principal component, which in our experiments were assigned to pure $CaCO_3$ phases (i.e., calcite and ikaite). The loading vectors represent the contribution of a given phase at various reaction times. These contribution profiles were normalized against the overall peak area and the number of electrons per formula unit of ikaite and calcite, so that the ratio between both profiles was proportional to their molar ratio.

The final precipitates from the *in situ* and real-time experiments were separated from the solutions by using vacuum filtration, then rinsed with isopropanol to remove remaining water, and quickly dried by blowing air over the solids. Powder X-ray diffraction (XRD, Bruker D8, Co K$\alpha_{1,2}$ radiation, 0.02° from 10 to 70° 2θ, 1° min^{-1}) was used to verify the nature of the $CaCO_3$ phases present at the end of the experiment, while scanning electron microscopy (SEM, FEI Quanta 3D, 5 kV) and transmission electron microscopy (TEM, Phillips CM 20, 20 kV) were utilized to characterize their crystal size and morphology.

RESULTS AND DISCUSSION

For the tested CIT/Ca ratios, ACC formed within the first 30 s after solution mixing as indicated by the sharp increase to $I \propto q^{-4}$ in the SAXS intensity in the low-q regime (for $q < 1$ nm^{-1} Figure 1B) and the absence of any crystalline phases in the WAXS pattern (Figure 1C). Since this curve does not level off for lower q-values within the measured range, the particles within these suspensions must have reached particle radii larger than 50 nm ($\approx \pi/q_{min}$). XRD analyses performed on these initial precipitates (prepared offline, under identical conditions) confirmed that the ACC material was characterized only by the presence of broad correlation peaks in the patterns.

The so-formed ACC remained stable for approximately 20 min prior to crystalline $CaCO_3$ formation. From our previous work,[23] we had expected that in the presence of CIT, ACC would crystallize directly to calcite, which indeed we observed for the 50% CIT/Ca experiment (Figure 2A). However, in the 100% CIT/Ca experiment, the time-resolved WAXS pattern (Figure 1C) showed the presence of two separate crystalline phases distinguished by the PCA analyses that could be assigned to ikaite (Figure 1C−I) and calcite (Figure 1C−II), respectively. In this experiment, we observed the formation of ikaite at $t = 20$ min (Figures 1C and Figure 2A), when ACC presumably started to dissolve.[29] Once formed, Ikaite continued to increase in volume fraction up to $t = 30$ min,

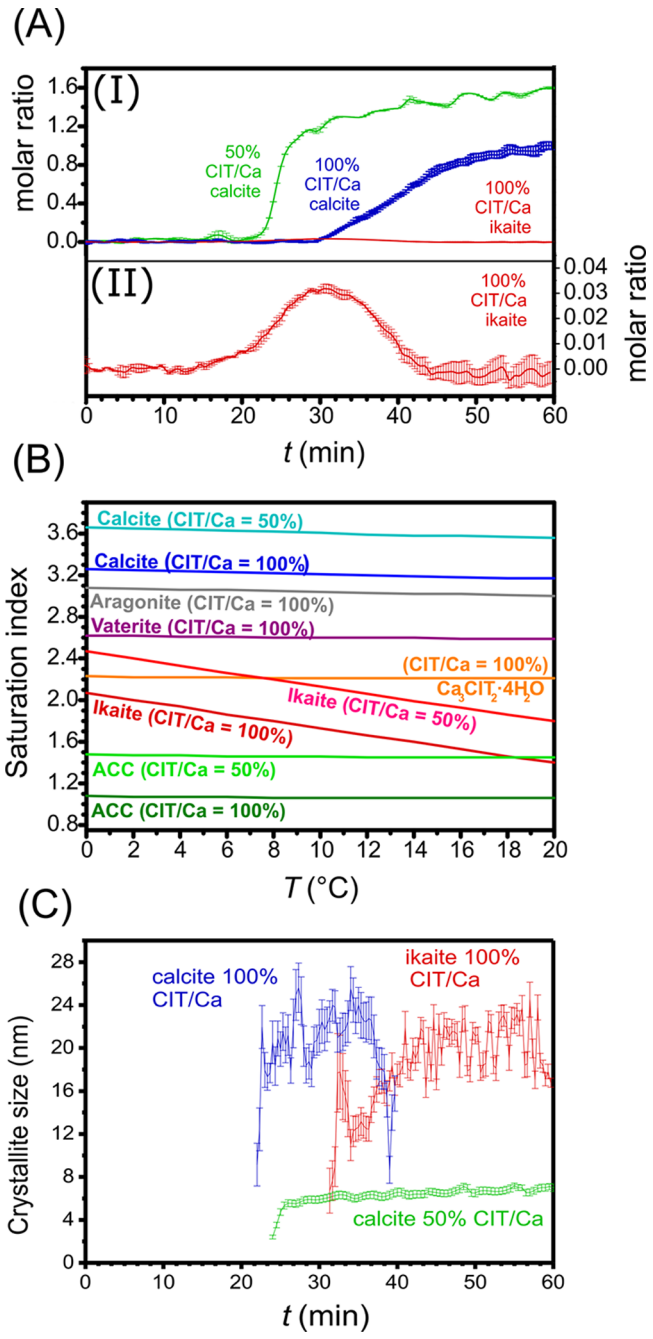

Figure 2. (A-I) Time resolved molar ratios of ikaite and calcite for both 50% and 100% CIT/Ca, with respect to 100% CIT/Ca at $t = 60$ min. This was quantified by multiplying the contribution of a given principal component with the WAXS peak areas of the corresponding principal component, subsequently normalized against the number of moles electrons per molar unit of a given polymorph, and finally normalized against 100% CIT/Ca at $t = 60$ min. (A-II) Amplified graph for the molar ratio of ikaite for 100% CIT/Ca. (B) Saturation indices for calcium carbonate polymorphs and $Ca_3CIT_2{\cdot}4H_2O$. Saturation indices were calculated with PHREEQC[30] by using temperature-dependent solubility products for calcite, vaterite, and aragonite from ref 31 and for ACC from ref 32. (C) Crystallite size of calcite for both 50 and 100% CIT/Ca (PC1) and ikaite for 100% CIT/Ca (PC2) by using the Scherrer equation obtained from the time-resolved WAXS patterns.

after which calcite started to appear (Figures 1C and Figure 2A). Thereafter, calcite steadily increased in its volume fraction

DOI: 10.1021/acs.cgd.7b00743
Cryst. Growth Des. 2017, 17, 6224−6230

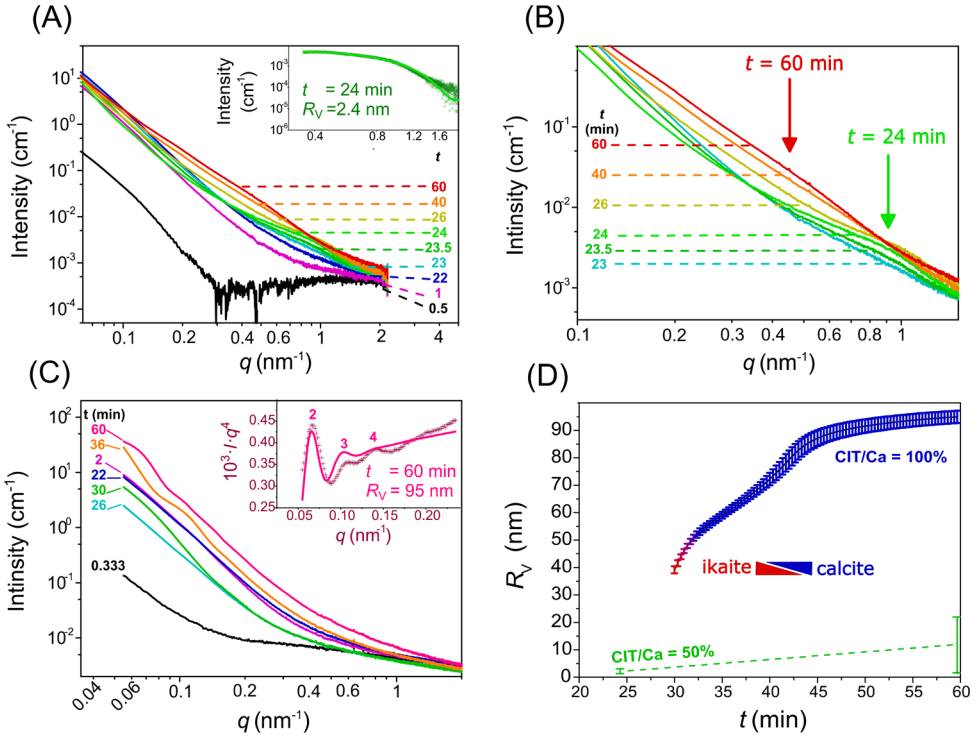

Figure 3. (A) This procedure revealed the presence of small solid particles with a radius R_V = 2.4 nm, (B) zoom in of SAXS pattern to emphasize the shift in the lobe to lower q-values for increasing reaction times; the green and red arrows point to the bending point of lobes for t = 23.5 and 60 min, respectively. (C) Selected SAXS patterns at various times after mixing for the 50% CIT/Ca experiment: the inset shows a SAXS pattern derived for the data at t = 24 min, from which the scattering at t = 22 min was subtracted, and this curve was fitted with a spherical form function, which included polydispersity with the Schultz−Zimm distribution.[34] (D) Volume averaged particle size, R_V, obtained from time resolved SAXS patterns.

concomitant with the decrease in ikaite volume fraction. This decrease lasted until t = 42 min, after which no more ikaite was detected. Nevertheless, calcite further increased in its volume fraction until t = 60 min. The matrix contribution profiles of calcite and ikaite (as obtained from PCA, Figure 1C−III and Figure 2A-III) were normalized against the overall peak area and the number of electrons per formula unit, so that the ratio between both profiles was proportional to their molar ratio.

Consequently, the maximum molar fraction of ikaite present at t = 30 min could be estimated to be approximately 3% of the final amount of calcite (at t = 60 min). Moreover, by comparing the changes in molar ratios between calcite and ikaite (Figure 2A), we could estimate the percentage of calcite that formed directly as a result of the breakdown of ikaite. If we consider the 10 time frames spanning t = 35 and 40 min, we observe that the maximum rate of ikaite depletion is still 15 times lower than the rate of calcite formation. In terms of molar ratios, only 6.4% of the $CaCO_3$ used for calcite formation was derived from ikaite, while the remaining 93.6% formed either from ACC or from the remnant supersaturated ions in the reacting solution.

A comparison between both experiments revealed a three times larger initial rate of calcite formation for the 50% CIT/Ca ratio compared to the 100% CIT/Ca experiment (Figure 2A). In part, this is explained by the difference in the saturation indices, which at T = 4 °C are 3.64 and 3.24 for calcite at CIT/Ca ratios of 50% and 100%, respectively (Figure 2B). Additionally, it has been shown that citrate slows down both calcite nucleation and growth kinetics through adsorption; thus at the higher citrate concentration, calcite crystallization was hindered to a larger extent, leading to a slower calcite crystallization rate. In addition, the calcite crystallite sizes were smaller at 50% CIT/Ca ($L \approx 6$ nm) compared to 100% CIT/Ca ($L \approx 18$ nm, Figure 2C). This size difference may be explained by a reduced nucleation rate for an increased CIT/Ca ratio and/or a different crystallization mechanism at 100% CIT/Ca, given the presence of ikaite. Although the presence of citrate reduce calcite crystallization rates, this does not affect the calcite crystal size, as shown in recent work.[33] Calcite crystals became more elongated with increasing CIT/Ca, showing preferential growth in one direction due to citrate adsorption at $\{10\bar{1}4\}$ steps, while the crystal volume remained constant.

As mentioned above, no ikaite peaks were detected in WAXS patterns of the 50% CIT/Ca experiment. The direct transition from ACC to calcite is likely a result of ACC dissolution and nucleation and growth of calcite from solution. This is also suggested by the SAXS pattern from this experiment (Figure 3A), which showed the appearance of a new lobe with a bending or knee point at $q \approx 0.8$ nm^{-1} for t = 24 min. This is indicative of an additional nucleation event, which in this experiment coincides with the nucleation of calcite. Fitting of this lobe revealed a volume averaged spherical particle radius of R_V = 2.4 nm at t = 24 min (inset in Figure 3A). This size may be close to the critical nucleus size of calcite, which seems consistent with molecular dynamic calculations, which suggested that at a diameter below 3.8 nm calcite becomes thermodynamically unfavorable with respect to ACC with an optimal hydration ratio.[35] As crystallization continues, these particles increased both in size and polydispersity as shown by the shift to lower q-values and the broadening of the lobe (see arrows Figure 3B).

One second before the onset of calcite crystallization at t = 30 min for the 100% CIT/Ca experiment, a lobe with a

DOI: 10.1021/acs.cgd.7b00743
Cryst. Growth Des. 2017, 17, 6224−6230

bending point at $q \approx 0.075$ nm^{-1} appeared in SAXS pattern (Figure 3C), which corresponded to presumably ikaite particles with a size of $R_V \approx 40$ nm. We did not observe such particles in an earlier stage despite the fact that ikaite was already observed after 20 min, possibly due to an insufficient volume fraction of ikaite with respect to the ACC particle, that may dominate the SAXS patterns at earlier time frames. Moreover, these particles may be partially composed of ACC, but calcite was still absent at this stage.

For increasing reaction times, as ikaite transforms to calcite, this lobe shifted to lower q-values corresponding to increasing particle sizes, and lobes appeared in the patterns which positions corresponded to higher order oscillations of the same presumably spheroidal particles (see curve of t = 36 and 60 min Figure 3C and inlet). Meanwhile no new lobes appeared at lower q-range ($q > 0.2$ nm^{-1}) in this experiment at the onset of calcite formation. Thus, as calcite formed in the 100% CIT/Ca experiment, its particle size remained fairly large ($R_V > 40$ nm) compared to the 50% CIT/Ca experiment ($3 \leq R_V \leq 22$ nm) as illustrated in Figure 3D. The absence of distinct and separated calcite nuclei could indicate that the calcite grew on ikaite or ACC surfaces without a separating double layer. Complementary to these SAXS experiments, particle size and morphology were characterized ex-situ with SEM and TEM, and these results indicate that in the 50% CIT/Ca experiment, particle aggregates were more fine-grained (Figure 4A,B) and individual crystals were smaller (Figure 4C,D) compared to the 100% CIT/Ca.

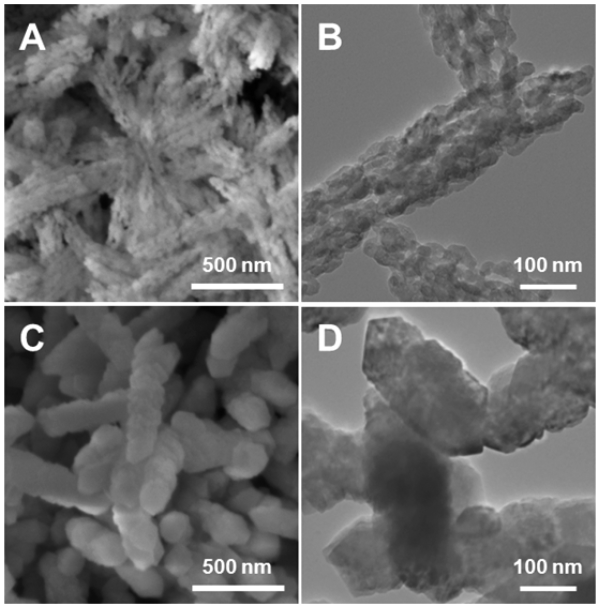

Figure 4. SEM (A) and TEM (B) of calcite formed after 2 h with 50% CIT/Ca, and SEM (C) and TEM (D) of calcite formed after 1 h with 100% CIT/Ca.

We summarized our findings in a schematic diagram (Figure 5). For both 50% and 100% CIT/Ca ratios, ACC aggregates with diameters larger than 100 nm formed almost instantaneously (Figure 5A). For the 50% CIT/Ca experiment, ACC transformed directly to calcite, without any other intermediate stages or any other metastable $CaCO_3$ phases (Figure 5B,C). In contrast in the 100% CIT/Ca experiment, metastable ikaite formed and this transformed to calcite (Figure 5D–F).

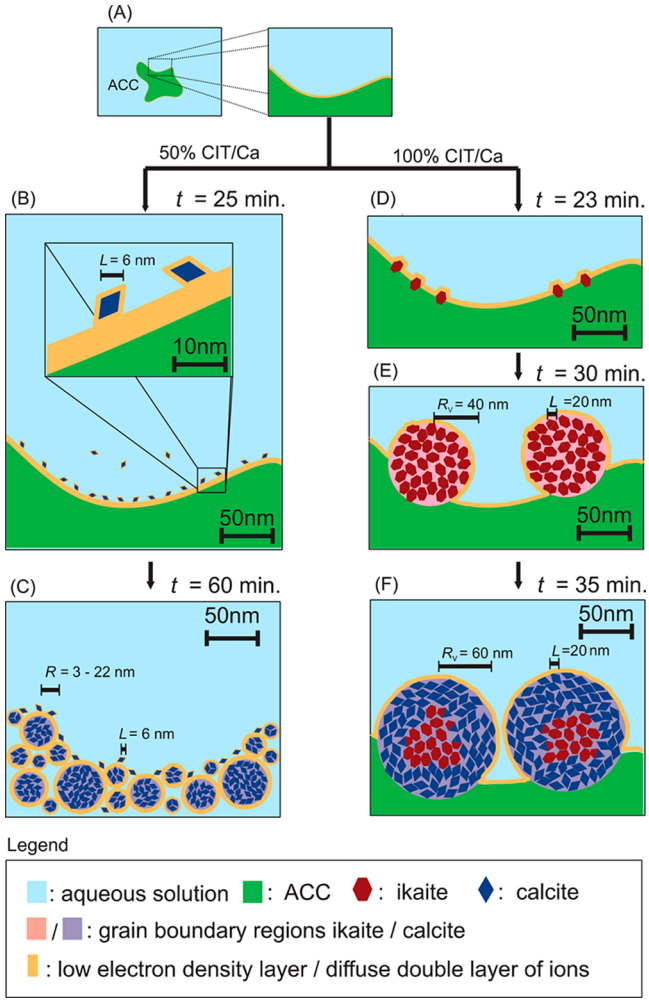

Figure 5. Illustration of particle formation for 50% and 100% CIT/Ca. (A) ACC particles were present immediately after mixing of the citrate/carbonate solution with the calcium solution for both CIT/Ca ratios. (B) In the 50% CIT/Ca experiment, nucleation of calcite nanoparticles was clearly visible in the SAXS pattern at 24 min. These calcite nanoparticles were potentially separated from the ACC particles by a low electron dense diffuse ion double layer, allowing them to be observed as individual entities within the SAXS pattern. (C) With time, a polydisperse mixture of calcite particles formed. No ikaite formed in this experiment. (D) In the 100% CIT/Ca, ikaite nanocrystallites formed at 23 min that could not be distinguished as individual nanoparticles within the SAXS pattern. (E) Fairly monodisperse particles of ikaite crystals at 30 min just before calcite nucleated. (F) Mixed ikaite/calcite particles at 35 min after mixing the solutions for 100% CIT/Ca.

The calcite that nucleated in the 50% CIT/Ca experiment formed as small nanoparticles as revealed by a small lobe in the SAXS pattern, which was clearly distinguished from its underlying baseline (Figure 3A,B). Because of the simultaneous particle growth and formation of new particle nuclei, the polydispersity increased (Figures 3D and Figure 5C), which explains the diminishing lobe in the SAXS curve (Figure 3B, from green arrow to red arrow).

On the contrary, in the 100% CIT/Ca experiment after ACC formation, only distinct nanoparticles of ikaite formed, and the degree of polydispersity was reduced as the ikaite particle sizes grew with time (see lobes in the SAXS pattern Figure 3C). This change became more pronounced as the reaction proceeded

DOI: 10.1021/acs.cgd.7b00743
Cryst. Growth Des. 2017, 17, 6224–6230

and the ikaite particles continued to grow, and eventually they started to transform after 30 min into calcite (Figure 5D−F). Important to note is the fact that calcite did not form separate particles, but the newly forming calcite crystals coexisted with ikaite particle (Figure 5F). Thus, ikaite and calcite likely grew on top of each other without diffuse double layers in between. This made it practically impossible to distinguish them as individual particles in the SAXS or WAXS data. In the end stages of the reaction, all ikaite particles transformed into fairly monodisperse calcite particles with an R_V = 95 nm. Noteworthy is that these sizes are roughly 8 times the sizes of the calcite particles that formed in the 50% CIT/Ca experiment (R_V = 3−22 nm).

In our experiment the ikaite-to-calcite transformation is more complex than in previously reported experiments, since ikaite was not the only source of $CaCO_3$ for calcite formation. The highest dissolution rate of ikaite was ∼15 times smaller than the calcite formation rate. Consequently, the majority of $CaCO_3$ for calcite formation originated from the dissolution of the initially formed ACC and/or from remnant ions in solution. The so-formed calcite and ikaite crystals are highly porous and similar to glendonite-type calcite polymorphs. Because of their high surface areas (see also Figure 4), such crystals are ideal seeds for further growth from Ca^{2+} and CO_3^{2-} in solution. Thus, even though ikaite was formed as a minor phase in our experiments, it acted as a seed crystal and likely played a crucial role in the calcite formation mechanism. The presence of such seeding crystallites facilitated the formation of enlarged calcite crystallites (L = 20 nm) at 100% CIT/Ca compared to the smaller calcite crystallite (L = 6 nm) at 50% CIT/Ca, where no ikaite formed. The increased calcite crystallite size for 100% CIT/Ca could potentially be explained by the increased solubility of calcite at the higher CIT/Ca ratio. However, previous experiments at 25 °C, where ACC transformed directly to calcite, without ikaite formation, revealed that the calcite crystallite size decreases with an increase in CIT/Ca ratio, due to an increasing calcite solubility.[23] This is the opposite trend to what is observed here at reduced temperatures, further supporting that the presence of ikaite affected the final calcite crystallite size by acting as seeding material.

As proposed by Sanchez-Pastor et al.[18] the pseudomorphic ikaite-to-calcite transition may occur through an interface-coupled dissolution reprecipitation mechanism. However, our SAXS experiments did not provide any indication of the existence of a low electron density liquid-like interface that separates the calcite from the ikaite phase and facilitated its transformation mechanism. If such a liquid interface existed, its electron density must be close to the electron density of ikaite, as otherwise the SAXS-curves should provide evidence of its existence. Possibly, such liquid interfaces may exist, but with a similar composition and consequently a similar electron density as ikaite. This could mean that ikaite first melts to a highly supersaturated solution of 1 mol of $[Ca^{2+}{\cdot}CO_3^{2-}]$ per 6 mol of H_2O, which subsequently immediately recrystallized into calcite. There is probably no need for additional water to be present at the ikaite−calcite interface, since the liquid interface can have the same composition as ikaite. This is consistent with previous research showing that no additional water was required for the ikaite-to-calcite transformation.[18] On the other hand, the available amount of water in ACC is substantially lower (typically $CaCO_3{\cdot}1\ H_2O$). As a result the liquid interface between ACC and calcite probably contains a higher water content than the adjacent ACC and calcite, which provided a more distinct contrast between the solids and the electron poor interface that separated them. As a consequence we can observe the formation of separated calcite nanoparticles in the 50% CIT/Ca experiment (in the absence of ikaite) with a distinct diffuse double layer, which had not been observed for the 100% CIT/Ca experiment.

CONCLUSIONS

As shown before, calcite crystallization was retarded in the presence of citrate as a complexing/coordinating ligand in solution and consequently enhancing the lifetime of amorphous calcium carbonate (ACC). In the 50% CIT/Ca experiment, nanosized calcite entities (R_V = 2.4 nm, L = 2.3 nm) nucleated after 22 min, which were seeding a fine-grained spherulitic calcite morphology with aggregated particles in a size range between 3.5 < R < 22 nm being composed of crystallites with a size of typically $L \approx 6$ nm.

At 100% CIT/Ca, ikaite formed concomitant with ACC dissolution and prior to calcite formation. Its formation was facilitated by the low temperature conditions, and the presence of chelating citrate ligands that are analogous to phosphate ligands retards the formation of anhydrous $CaCO_3$. However, given the substantially lower transformation rate of ikaite versus the formation rate of calcite, it seems that only a minority (max 6.4%) of calcite was formed via ikaite as an intermediate. On the other hand, the pseudomorphic ikaite-to-calcite transition provides porous calcite crystals (glendonite polymorph) being ideal (high-surface area) seeding crystal for further crystallization from solution.

The mechanism of calcite formation with a 100% CIT/Ca ratio is strikingly different as compared to the 50% CIT/Ca ratio. Unlike the 50% ratio, the 100% ratio did not reveal nucleation of nanosized calcite crystals (R_V = 2.4 nm), instead yielding substantially larger crystallite (L = 20 nm) and particle size (R_V = 95 nm). The enlarged calcite crystallite size of 100% CIT/Ca is most likely explained by the presence of glendonite (porous calcite form ikaite as a parent) that serves as seeding crystallites.

AUTHOR INFORMATION

Corresponding Author

*E-mail: dominique.tobler@nano.ku.dk.

ORCID

R. Besselink: 0000-0002-2027-9403

D. J. Tobler: 0000-0001-8532-1855

Notes

The authors declare no competing financial interest.

ACKNOWLEDGMENTS

This work was funded by the Engineering and Physical Sciences Research Council (EPSRC) program grant (EP/I001514/1) for the Materials Interface with Biology (MIB) Consortium. The synchrotron work was funded via Diamond Light Source (grant number SM9904) to J.D.R.B. J.D.R.B. and D.J.T. also acknowledge financial support by the NanoCArB (PIEFGA-2013-624016) and MIRO (PIEF-GA-2013-624619) Marie Curie Intra-European Fellowship (IEF), respectively. Moreover, this research was partially made possible by Marie Curie grant from the European Commission in the framework of NanoSiAl Individual Fellowship, Project No. 703015 to T.M.S. R.B., T.M. S. and L. G. B. acknowledge the financial support of

DOI: 10.1021/acs.cgd.7b00743
Cryst. Growth Des. 2017, 17, 6224−6230

the Helmholtz Recruiting Initiative. We are grateful to for the help provided by Dr. James Doutch on beamline I22.

REFERENCES

(1) Ridgwell, A.; Zeebe, R. E. *Earth Planet. Sci. Lett.* **2005**, *234*, 299−315.
(2) Tegetoff, F. W. *Calcium Carbonate*, 1st ed.; Birkhäuser: Basel, 2002.
(3) Rodriguez-Blanco, J. D.; Sand, K. K.; Benning, L. G. *In New Perspectives on Mineral Nucleation and Growth: From Solution Precursors to Solid Materials*; Van Driessche, A. E. S., Kellermeier, M., Benning, L. G., Gebauer, D., Eds.; Springer International Publishing: Cham, 2017; pp 93−111.
(4) Xiao, J.; Yang, S. *Nanoscale* **2012**, *4* (1), 54.
(5) Sand, K. K.; Rodriguez-Blanco, J. D.; Makovicky, E.; Benning, L. G.; Stipp, S. L. S. *Cryst. Growth Des.* **2012**, *12*, 842−853.
(6) Westin, K. J.; Rasmuson, A. C. *J. Colloid Interface Sci.* **2005**, *282* (2), 359−369.
(7) de Leeuw, N. H.; Parker, S. C. *J. Chem. Soc., Faraday Trans.* **1997**, *93* (3), 467−475.
(8) Harris, J.; Mey, I.; Hajir, M.; Mondeshki, M.; Wolf, S. E. *CrystEngComm* **2015**, *17* (6831), 6767−7008.
(9) Beck, R.; Andreassen, J. *J. Cryst. Growth* **2010**, *312* (15), 2226−2238.
(10) Addadi, L.; Joester, D.; Nudelman, F.; Weiner, S. *Chem. - Eur. J.* **2006**, *12*, 980−987.
(11) Dauphin, Y.; Dufour, E. *Micron* **2008**, *39* (7), 891−896.
(12) Tseng, Y.; Chevallard, C.; Dauphin, Y.; Guenoun, P. *CrystEngComm* **2014**, *16*, 561−569.
(13) Gower, L. A.; Tirrell, D. A. *J. Cryst. Growth* **1998**, *191*, 153−160.
(14) Seto, J.; Ma, Y.; Davis, S. A.; Meldrum, F.; Gourrier, A.; Kim, Y.-Y.; Schilde, U.; Sztucki, M.; Burghammer, M.; Maltsev, S.; Jäger, C.; Cölfen, H. *Proc. Natl. Acad. Sci. U. S. A.* **2012**, *109* (10), 3699−3704.
(15) Shearman, D. J.; Smith, A. J. *Proc. Geol. Assoc.* **1985**, *96* (4), 305−314.
(16) Swainson, I. P.; Hammond, R. P. *Mineral. Mag.* **2003**, *67* (3), 555−562.
(17) De Lurio, J. L.; Frakes, L. A. *Geochim. Cosmochim. Acta* **1999**, *63* (7−8), 1039−1048.
(18) Sánchez-Pastor, N.; Oehlerich, M.; Astilleros, J. M.; Kaliwoda, M.; Mayr, C. C.; Fernández-Díaz, L.; Schmahl, W. W. *Geochim. Cosmochim. Acta* **2016**, *175*, 271−281.
(19) Hellenbrandt, M. *Crystallogr. Rev.* **2004**, *10* (1), 37−41.
(20) Downs, R. T.; Hall-Wallace, M. *Am. Mineral.* **2003**, *88*, 247−250.
(21) Rickaby, R. E. M.; Shaw, S.; Bennitt, G.; Kennedy, H.; Zabel, M.; Lennie, A. *Geology* **2006**, *34* (6), 497−500.
(22) Rodriguez-Blanco, J. D.; Shaw, S.; Bots, P.; Benning, L. G.; Roncal-Herrero, T. *J. Alloys Compd.* **2012**, *536* (1), S477−S479.
(23) Tobler, D. J.; Rodriguez-Blanco, J. D.; Dideriksen, K.; Bovet, N.; Sand, K. K.; Stipp, S. L. S. *Adv. Funct. Mater.* **2015**, *25* (20), 3081−3090.
(24) Mueller, M.; Wang, M.; Schulze-Briese, C. G. *Acta Crystallogr., Sect. D: Biol. Crystallogr.* **2012**, *68* (1), 42−56.
(25) Huang, T. C.; Toraya, H.; Blanton, T. N.; Wu, Y. *J. Appl. Crystallogr.* **1993**, *26* (2), 180−184.
(26) Fratzl, P.; Misof, K.; Zizak, I.; Rapp, G.; Amenitsch, H.; Bernstorff, S. *J. Struct. Biol.* **1998**, *122* (1), 119−122.
(27) Zhang, F.; Ilavsky, J.; Long, G. G.; Quintana, J. P. G.; Allen, A. J.; Jemian, P. R. *Metall. Mater. Trans. A* **2010**, *41* (5), 1151−1158.
(28) Guinier, A. X-ray Diffraction. In *Crystals, Imperfect Crystals, and Amorphous Bodies*; Dover Publications, Inc.: New York, 1994.
(29) Bots, P.; Benning, L. G.; Rodriguez-Blanco, J.-D.; Roncal-Herrero, T.; Shaw, S. *Cryst. Growth Des.* **2012**, *12* (7), 3806−3814.
(30) Parkhurst, D. L.; Appelo, C. A. J. *Description of Input and Examples for PHREEQC version 3—A Computer Program for Speciation, Batch-Reaction, One-Dimensional Transport, and Inverse Geochemical Calculations*; U.S. Geological Survey Techniques and Methods, 2013, https://pubs.usgs.gov/tm/06/a43/.
(31) Plummer, L. N.; Busenberg, E. *Geochim. Cosmochim. Acta* **1982**, *46* (6), 1011−1040.
(32) Brecevic, L.; Nielsen, A. E. *J. Cryst. Growth* **1989**, *98* (3), 504−510.
(33) Montanari, G.; Rodriguez-Blanco, J. D.; Bovet, N.; Stipp, S. L. S.; Tobler, D. J. *Cryst. Growth Des.* **2017**, DOI: 10.1021/acs.cgd.7b00796. 10.1021/acs.cgd.7b00796
(34) Kotlarchyk, M.; Chen, S.-H. *J. Chem. Phys.* **1983**, *79* (5), 2461.
(35) Raiteri, P.; Gale, J. D. *J. Am. Chem. Soc.* **2010**, *132* (6), 17623−17634.

DOI: 10.1021/acs.cgd.7b00743
Cryst. Growth Des. 2017, 17, 6224−6230